Analysis of Ultrasonic Wave Dispersion in Presence of Attenuation and Second Gradient Contributions

Nicola De Fazio *, Luca Placidi, Francesco Fabbrocino, Raimondo Luciano

Posted Date: 1 April 2025

doi: 10.20944/preprints202504.0083.v1

Keywords: ultrasonic wave dispersion; second-gradient theory; attenuation

 doi:10.20944/preprints202504.0083.v1

Article

Analysis of Ultrasonic Wave Dispersion in Presence of Attenuation and Second Gradient Contributions

Nicola De Fazio [1,*,‡], Luca Placidi [2,‡], Francesco Fabbrocino [3,‡] and Raimondo Luciano [4,‡]

[1] University of Catania, Engineering Faculty, Piazza Università, 2, 95124 Catania
[2] International Telematic University Uninettuno, Engineering Faculty, Corso Vittorio Emanuele II, 39, 00186 Roma
[3] Pegaso Telematic University, Engineering Faculty, Centro Direzionale Isola F2 - Napoli
[4] Parthenope University of Naples, Engineering Faculty, Via Ammiraglio Ferdinando Acton, 38, 80133 Napoli
* Correspondence: nicola.defazio@phd.unict.it
‡ These authors contributed equally to this work.

Abstract: In this study, we aim to analyze ultrasonic wave dispersion equation due to second-gradient contributions and attenuation within the framework of continuum mechanics. To analyze dispersive behavior and attenuation effects, we consider the influence both of higher-order gradient terms (second gradients) and of viscoelastic contributions of Rayleigh type. To this end, we use the extended Rayleigh-Hamilton principle to derive the governing equations of the problem. Using a wave-form solution, we establish the relationship between phase velocity and the material's constitutive parameters, including those related to stiffness of first (standard) and of second-gradient type, and to viscosity. To validate the model, we use data available in the literature to provide a possible identification of all the material parameters. Thus, for the same identification, we observe that our model provides a good approximation of the experimentally measured trends of both the phase velocity and the attenuation vs frequency. In conclusion, this result not only confirms that our model can accurately describe both wave dispersion and attenuation in a material, as observed experimentally, but also highlights the necessity of simultaneously considering both second-gradient and viscosity parameters for a proper mechanical characterization of materials.

Keywords: ultrasonic wave dispersion; second-gradient theory; attenuation

1. Introduction

Ultrasonic wave propagation is a powerful technique used in a wide range of fields, from non-destructive testing (NDT) and material characterization to medical diagnostics. The study of how ultrasonic waves behave as they travel through materials provides essential information about the internal structure and mechanical properties of the materials being tested. In traditional models, wave propagation is typically described using classical elasticity theory, where the stress-strain relationship of the material depends on the first derivatives of the displacement field, representing the strain. Although this approach works well for simple, homogeneous materials, it is insufficient for more complex materials that possess microstructural heterogeneity or exhibit non-local interaction, since these materials often exhibit non-local behavior, meaning that the response at any given point in the material is influenced not only by the immediate surroundings but also by broader microstructural features. Second-gradient elasticity theory was developed to address this issue by introducing higher-order derivatives of the displacement field, which enables the model to capture these non-local effects and internal length scales within the material. Then, this theory has become particularly useful for modeling materials that exhibit scale-dependent behavior, such as foams, granular materials, and biological tissues. By incorporating second-gradient terms into the stress-strain relationship, this theory provides a more accurate description of wave propagation in materials with microstructural features, where the classical theory would not capture the complex interactions between the structure of the material and the propagating wave [1,2].

 doi:10.20944/preprints202504.0083.v1

Dispersion refers to the phenomenon in which the speed of a wave depends on its frequency. In most classical wave propagation theories, the velocity of the wave is constant and independent of frequency. However, in second-gradient media, the wave velocity is frequency-dependent. This is because the material's internal structure, captured e.g. by the second-gradient terms, affects the wave's propagation at different frequencies. This effect can be especially pronounced in materials where microstructural characteristics, such as pores, inclusions, or heterogeneity, influence wave propagation [3,4]. In practice, the dispersion observed in second-gradient media can lead to significant differences in how waves propagate, especially at higher frequencies. This has important implications for the design and analysis of materials such as metamaterials, where customizable dispersion characteristics are often desired to achieve specific effects, such as negative refraction or slow-wave propagation [5]. Similarly, in biological tissues, where wave dispersion is influenced by the cellular structure of the tissue, understanding dispersion becomes critical to improving medical imaging techniques such as ultrasound elastography [6].

Attenuation refers to the loss of energy that occurs when a wave propagates through a medium. In traditional wave theory, attenuation is typically associated with damping mechanisms, such as viscoelastic effects or material imperfections. However, in materials exhibiting second-gradient behavior, attenuation can arise due to the non-local interactions and microstructural features that influence wave propagation. As ultrasonic waves pass through a material with second-gradient effects, their energy is dissipated in a way that cannot be fully explained by classical damping models [7,8]. The attenuation in such materials is also frequency-dependent, with the energy loss being more significant at higher frequencies. This frequency-dependent attenuation is crucial for understanding wave behavior in biological tissues, where the microstructural properties of the tissue (such as cellular arrangements) can cause additional dissipation of wave energy. Similarly, in porous materials and composites, where waves interact with heterogeneities at multiple scales, the attenuation behavior provides valuable insight into the material's internal structure and mechanical properties [9].

The theoretical framework of second-gradient elasticity, which includes both dispersion and attenuation effects, has several important applications. Understanding the frequency-dependent dispersion and attenuation can enhance the sensitivity and resolution of ultrasonic testing techniques, allowing for better detection of defects, cracks, or voids within materials [9]. In medical diagnostics, particularly in ultrasound elastography, these models can provide a more accurate representation of wave propagation through biological tissues. Since tissues often exhibit complex internal structures, the ability to account for non-local effects and microstructural interactions improves the precision of measurements, leading to more reliable assessments of tissue stiffness or elasticity. This has important implications for early diagnosis and monitoring of conditions such as tumors or liver fibrosis [6]. Additionally, the study of second-gradient effects in ultrasonic wave propagation is crucial for the development of metamaterials, engineered materials designed to have specific wave propagation characteristics. By tailoring the second-gradient parameters, researchers can design materials with bespoke dispersion and attenuation properties, opening up new possibilities for applications in sensing, communication, and imaging technologies [5]. Last but not least, we would like to highlight a recent contribution that has significantly inspired our work, specifically the thesis by Ronny Hofmann[10]. His study focuses on laboratory measurements of clastic rocks, ranging from 3 Hz to 500 kHz, and their application to well log analysis and a time-lapse study in the North Sea. Within this framework, the measurements reveal substantial dispersion in sandstones due to the saturation of inhomogeneities and open boundaries (such as pore pressure diffusion), which in turn affects the material's compressibility and stiffness.

Furthermore, attenuation is directly related to the rate of change of the modulus. This concept is summarized in Figure 1 [10], which illustrates that a certain parameter μ defined in Hofmann's thesis [10] changes i.e. from 0.8 to 0.2, the dispersion of phase velocities is higher as Figure 1a and the attenuation peaks in Figure 1b become more pronounced. The variation of phase velocity occurs at peak attenuation frequency, as for Figure 1c.

 doi:10.20944/preprints202504.0083.v1

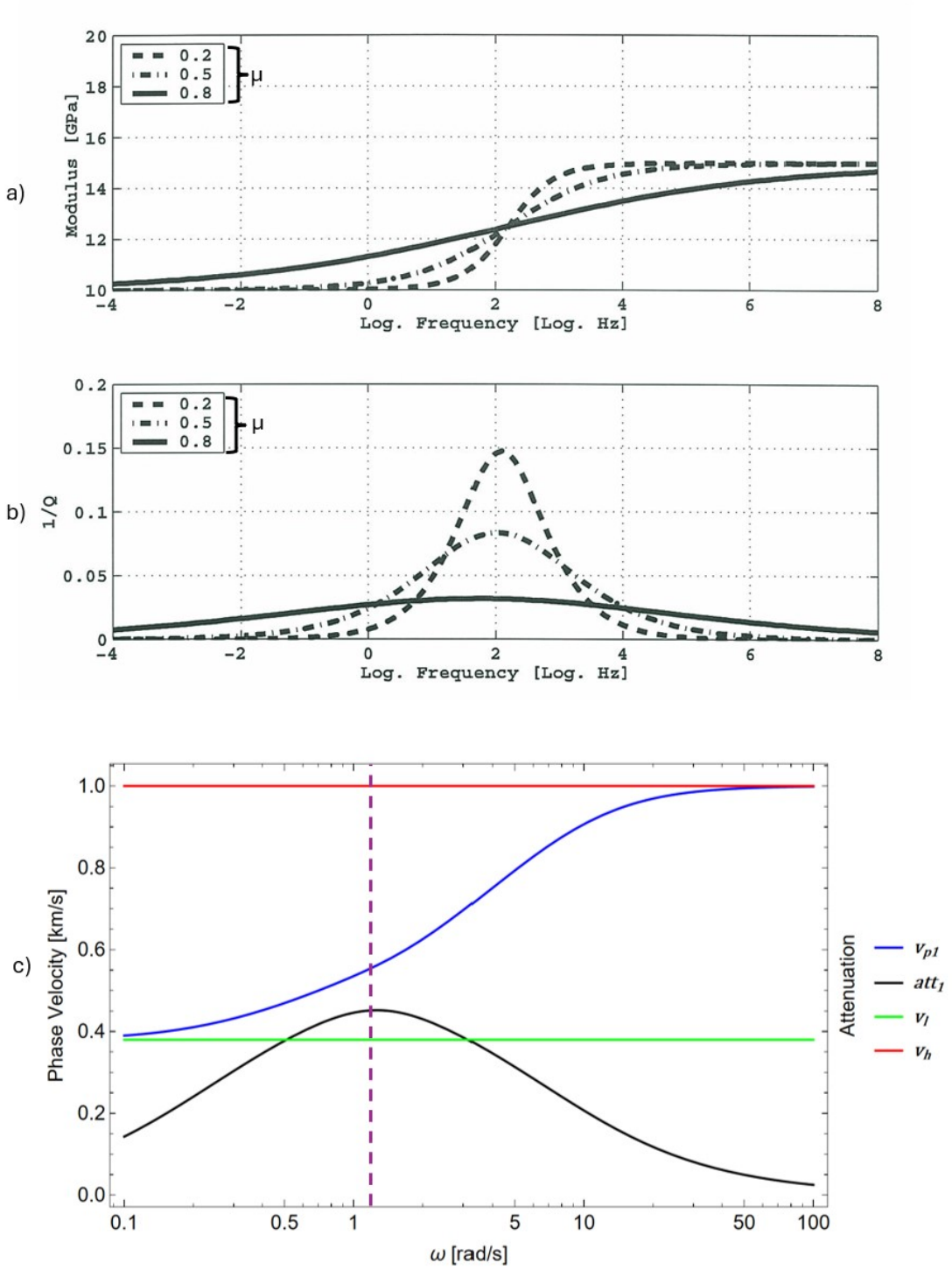

Figure 1. *Influence of a certain parameter μ defined in Hofmann's thesis [10] on phase velocity (a) and attenuation (b).In the attenuation peak point we observe the variation of phase velocity (c).*

Since no continuous model currently exists that can capture the aforementioned effect, the aim of this research is to provide a model that, starting from the Rayleigh-Hamilton principle and considering both the material's internal viscosity and second-gradient parameters, can simulate the aforementioned dispersive and dissipative effects.

Beside the Introduction, the paper is organized into the following sections:

- Section 2 outlines the construction of the governing equations based on the Hamilton-Rayleigh principle, considering both internal viscosity and second gradient parameters of the material.

 doi:10.20944/preprints202504.0083.v1

Starting from the dispersion equation and using the wave form solution we derive the wavenumber, then the velocity phase and the quality factor for the evaluation of attenuation phenomena. Once the methodology and model have been finalized, we search for materials and experimental data from the literature to validate the model.

- Section 3 focuses on the validation of the above model. Three case studies from the literature (one involving natural materials and two involving artificial materials) are examined. The purpose is to compare experimental data with the numerical simulation results derived from the model. Results and comments on the comparison above mentioned are also discussed in this section. Moreover, we have introduced a numerical simulation to evaluate general aspects of the wave's behavior, both from the perspective of dispersion and attenuation.
- Finally, Section 4 offers our conclusions, reflections on future developments and reports all the contributions.

A list of abbreviations used in the manuscript and all the references adopted for this study are presented at the end of the article.

2. Modelling and Methods

2.1. Scope and Strategy

We are searching for a model that can reproduce the variation of phase velocity and attenuation with wave frequency for a given material, as shown in Figure 1c, that is our benchmark. In this context, we will consider the Rayleigh-Hamilton principle, using second-gradient and viscous parameters to describe the displacement involved in the energies represented in the principle. The Partial Differential Equation (PDE) obtained will be solved using a wave form solution to derive the dispersion equation that includes phase velocity and attenuation.

2.2. Variational Derivation of Governing Equations (PDE and BCs)

We begin by recalling the extended Rayleigh-Hamilton principle that postulates the variation of the Action, δA, to be connected to the Rayleigh function R:

$$\delta A = \int_{t_0}^{t_1} \left\{ \int_0^L \left(\delta K - \delta W^{\text{int}} \right) dx + \delta W^{\text{ext}} \right\} dt = \int_{t_0}^{t_1} \left(\frac{\delta R}{\delta \dot{u}'} \delta u' + \frac{\delta R}{\delta \dot{u}''} \delta u'' \right) dt, \tag{1}$$

where the three energy functions K, the kinetic energy density, W, the potential energy density, and W^{ext}, the external energy function, are equal to:

$$K = \int_0^L \left(\frac{1}{2} \rho \dot{u}^2 + \frac{1}{2} \eta \dot{u}'^2 \right) dx, \tag{2}$$

$$W^{\text{int}} = \int_0^L \left(\frac{1}{2} k_1 u'^2 + \frac{1}{2} k_2 u''^2 \right) dx, \tag{3}$$

$$W^{\text{ext}} = \left[F_0^{\text{ext}} u + B_0^{\text{ext}} u' \right]_{x=0} + \left[F_L^{\text{ext}} u + B_L^{\text{ext}} u' \right]_{x=L} + \int_0^L \left(b_n u + b_d u' \right) dx, \tag{4}$$

and the Raylegh function is:

$$R = \int_0^L \left(\frac{1}{2} c_1 \dot{u}'^2 + \frac{1}{2} c_2 \dot{u}''^2 \right) dx \tag{5}$$

We recall that k_1 and k_2 are the standard elastic modulus for a linear one-dimensional elastic body and the non-standard strain-gradient modulus, respectively; given the displacement u, its derivatives with respect to time are denoted by $\dot{u}$ and with respect to space u' (first derivative) or u'' (second derivative), ρ and η are the mass density (mass per unit length) and the micro-inertia of the mono-dimensional body, respectively; b_n and b_d are the external distributed (per unit length) forces and double forces, respectively; F_0^{ext} (or F_L^{ext}) and B_0^{ext} (or B_L^{ext}) are the concentrated forces and double forces, evaluated at the extrema at $x = 0$ (or at $x = L$) of the one-dimensional body, respectively.

 doi:10.20944/preprints202504.0083.v1

Meanwhile, in the Raylegh function two internal viscosity are present,c_1 related to first gradient field and c_2 related to second gradient field.

Replacing (2), (3), (4) and (5) in the left side of equation (1) and integrating by parts, for every admissible variation of the displacement filed, the variation of the Action, δA, can be reduced to:

$$\begin{aligned}\delta A = &\int_{t_0}^{t_1}\left\{\int_0^L\left[\delta u\left(-\rho\ddot{u}+k_1u''+\eta\dot{u}''-k_2u^{(4)}+b_n-b_d'\right)\right]dx\right\}\\ &-\int_{t_0}^{t_1}\delta u(x=0)\left[-\eta\dot{u}'(x=0)-k_1u'(x=0)+k_2u'''(x=0)+b_d\right]dt\\ &+\int_{t_0}^{t_1}\delta u(x=L)\left[-\eta\dot{u}'(x=L)-k_1u'(x=L)+k_2u'''(x=L)+b_d\right]dt\\ &-\int_{t_0}^{t_1}\delta u'(x=0)\left[-k_2u''(x=0)\right]dt\\ &+\int_{t_0}^{t_1}\delta u'(x=L)\left[-k_2u''(x=L)\right]dt.\end{aligned} \tag{6}$$

The variation of Raylegh function will be:

$$\int_{t_0}^{t_1}\left(\frac{\delta R}{\delta\dot{u}'}\delta u'+\frac{\delta R}{\delta\dot{u}''}\delta u''\right)dt=\int_0^t\int_0^L\left(c_1\dot{u}'\delta u'+c_2\dot{u}''\delta u''\right)dx\,dt, \tag{7}$$

that integrating by parts, in space and time, becomes:

$$\begin{aligned}\int_{t_0}^{t_1}\left(\frac{\delta R}{\delta\dot{u}'}\delta u'+\frac{\delta R}{\delta\dot{u}''}\delta u''\right)dt=&\int_{t_0}^{t_1}\left[c_1\dot{u}'\delta u\right]_0^L dt-\int_{t_0}^{t_1}\int_0^L c_1\dot{u}''\delta u\,dx\,dt\\ &+\int_{t_0}^{t_1}\left[c_2\dot{u}''\delta u'\right]_0^L dt-\int_{t_0}^{t_1}\left[c_2\dot{u}'''\delta u\right]_0^L dt\\ &+\int_{t_0}^{t_1}\int_0^L c_2\dot{u}^{(4)}\delta u\,dx\,dt.\end{aligned} \tag{8}$$

Then, replacing equations (8) and (6) in (1) and ordering we obtain:

$$\begin{aligned}\delta A = &\int_{t_0}^{t_1}\left\{\int_0^L\left[\delta u\left(-\rho\ddot{u}+k_1u''+\eta\dot{u}''-k_2u^{(4)}+b_n-b_d'+c_1\dot{u}''-c_2\dot{u}^{(4)}\right)\right]dx\right\}dt\\ &-\int_{t_0}^{t_1}\delta u(x=0)\left[-\eta\dot{u}'(x=0)-k_1u'(x=0)+k_2u'''(x=0)+b_d\right.\\ &\qquad\left.-c_1\dot{u}'(x=0)+c_2\dot{u}'''(x=0)\right]dt\\ &+\int_{t_0}^{t_1}\delta u(x=L)\left[-\eta\dot{u}'(x=L)-k_1u'(x=L)+k_2u'''(x=L)+b_d\right.\\ &\qquad\left.-c_1\dot{u}'(x=L)+c_2\dot{u}'''(x=L)\right]dt\\ &-\int_{t_0}^{t_1}\delta u'(x=0)\left[-k_2u''(x=0)-c_2\dot{u}''(x=0)\right]dt\\ &+\int_{t_0}^{t_1}\delta u'(x=L)\left[-k_2u''(x=L)-c_2\dot{u}''(x=L)\right]dt=0.\end{aligned} \tag{9}$$

where, since the displacement $u(x,t)$ is assumed to be prescribed both at $t=t_0$ and at $t=t_1$, we have that $\delta u(x,t=t_0)=\delta u(x,t=t_1)=0$. Equation (9) must hold for every admissible variation δu of the displacement field u. So, the last four addends of equation (9) must therefore be null. On one hand, if the displacement u or the displacement gradient u' are prescribed at the boundary (i.e., the left-hand sides of the following equations are satisfied), then its variation is null as well as the corresponding line of equation (9). On the other hand, to make null the same lines of equation (9),

 doi:10.20944/preprints202504.0083.v1

if the mentioned kinematic conditions are not prescribed, then the right-hand sides of the following equations are satisfied:

$$\begin{aligned} & u(0,t) = u_0(t) \\ \text{or} \quad & -\eta\dot{u}'(x=0,t) - k_1 u'(x=0,t) + k_2 u'''(x=0,t) + b_d \\ & -c_1\dot{u}'(x=0,t) + c_2\dot{u}'''(x=0,t) = F_0^{\text{ext}}, \end{aligned} \tag{10}$$

$$\begin{aligned} & u(L,t) = u_L(t) \\ \text{or} \quad & -\eta\dot{u}'(x=L,t) - k_1 u'(x=L,t) + k_2 u'''(x=L,t) + b_d \\ & -c_1\dot{u}'(x=L,t) + c_2\dot{u}'''(x=L,t) = -F_L^{\text{ext}}, \end{aligned} \tag{11}$$

$$u'(0,t) = b_0(t) \qquad \text{or} \quad -k_2 u''(x=0,t) - c_2\dot{u}''(x=0,t) \quad = B_0^{\text{ext}}(t), \tag{12}$$

$$u'(L,t) = b_L(t) \qquad \text{or} \quad -k_2 u''(x=L,t) - c_2\dot{u}''(x=L,t) \quad = -B_L^{\text{ext}}(t). \tag{13}$$

for every instants of time, e.g., $\forall t \in \mathbb{R}$. Finally, also the first line of equation (9) must be zero for every admissible variation δu of the displacement field. Thus, because of its arbitrariness, it results:

$$-\rho\ddot{u} + k_1 u'' + \eta\ddot{u}'' - k_2 u^{(4)} - b_d' + b_n + c_1\dot{u}'' - c_2\dot{u}^{(4)} = 0, \quad \forall x \in [0,L], \quad \forall t \in \mathbb{R}. \tag{14}$$

2.3. Wave form solution

Equation (14) is the Partial Differential Equation (PDE) governing the evolution of the displacement field $u(x,t)$ for the investigated model, that will be solved in the following two subsections. In particular, we search for (14) a wave form solution and we assume the body length L to be sufficiently large so that the boundary conditions (BCs) (10)-(13) do not influence the solution.

Equation (14) can be solved considering no external distributed actions ($b_n = 0$ and $b_d = 0$) in the form of the following plane wave solution for the displacement field:

$$u(x,t) = \text{Re}\left(u_0 e^{i(\omega t - k_\omega x)}\right), \tag{15}$$

where u_0 is the complex wave amplitude, ω is the frequency of the wave expressed in Rad/s, k_ω is the complex wave number, i is the imaginary unit and Re is the real part operator. Calculating the derivatives of (15) and replacing them into (14), it results:

$$(k_2 + ic_2\omega)k_\omega^4 + (k_1 + ic_1\omega - \eta\omega^2)k_\omega^2 - \rho\omega^2 = 0, \tag{16}$$

where the arbitrariness of the complex wave amplitude u_0 has been considered. Equation (16) is a fourth-degree algebraic equation in terms of k_ω, and therefore admits four complex solutions for k_ω. However, in (16) k_ω appears only with even powers (k_ω^2 or k_ω^4). Thus, if $k_\omega = \hat{k}_\omega$ is a solution of (16) also $k_\omega = -\hat{k}_\omega$ is a solution as a consequence, then two of these solutions correspond to right-hand propagating waves, while the other two are equal in magnitude and opposite in sign. The reason is the isotropy of the domain. In the formulae, two independent solutions are:

$$k_{\omega_{1,2}} = \sqrt{\frac{-(k_1 + ic_1\omega - \eta\omega^2) \pm \sqrt{(k_1 + ic_1\omega - \eta\omega^2)^2 + 4(k_2 + ic_2\omega)(\rho\omega^2)}}{2(k_2 + ic_2\omega)}}. \tag{17}$$

 doi:10.20944/preprints202504.0083.v1

Remembering the correlation between frequency ω, wave number k_w and phase velocity v_p [11], we obtain an expression for the two phase velocities:

$$v_{p_{1,2}} = \mathrm{Re}\left(\frac{\omega}{k_{\omega_{1,2}}}\right) = \\ = \mathrm{Re}\left(\sqrt{\frac{2(k_2 + ic_2\omega)\omega^2}{-(k_1 + ic_1\omega - \eta\omega^2) \pm \sqrt{(k_1 + ic_1\omega - \eta\omega^2)^2 + 4(k_2 + ic_2\omega)(\rho\omega^2)}}}\right). \quad (18)$$

Similarly, starting from the wave number k_w, it is possible to determine the corresponding two quality factors Q_1 and Q_2 [10] as the inverse of the damping ratio *zeta*, then as a function of the real/imaginary parts of the wave number:

$$\zeta_{1,2} = \frac{1}{Q_{1,2}} = -\frac{\mathrm{Im}(k_{\omega_{1,2}})}{\mathrm{Re}(k_{\omega_{1,2}})}. \quad (19)$$

In conclusion, equations (18) and (19) serve as the reference for our model, linking phase velocity and attenuation to the frequency of the wave propagating through the material.

3. Validation: Results and Discussion

3.1. Introduction

As already highlighted in the introduction of this manuscript, we want to validate this model with data available for common construction material in the literature [12,13]. Such literature has been selected because, within many available articles, both phase velocity and attenuation measurements have been made for the same material at same frequencies. In detail, we investigate a sandstone sample [12], a cement paste sample [13]and finally a concrete sample [13]. For each material we have developed a case of study, then the validation is obtained by superimposing the theoretical predictions (obtained from numerical simulations) with the experimental data. In detail, first, we propose a numerical simulation that allows us to make general considerations about the dispersive behavior of the wave, characteristic of our model. Second, we validate the model using the materials presented above, comparing the available experimental data with the numerical simulation. The material constitutive parameters used in this section are presented in Table 1. Figures 2 and 3 refer to the numerical simulation toward the benchmark (Figure 1), while Figures 4–6 refer to the case studies.

Table 1. Table of constitutive parameters for different figures.

Reference	**Figure nr.**	**Constitutive Parameters**					
		k_1	k_2	ρ	η	c_1	c_2
		$[\mathrm{kg\,m^{-1}\,s^{-2}}]$	$[\mathrm{kg\,m\,s^{-2}}]$	$[\mathrm{kg\,m^{-3}}]$	$[\mathrm{kg\,m^{-1}}]$	$[\mathrm{kg\,m^{-1}\,s^{-1}}]$	$[\mathrm{kg\,m\,s^{-1}}]$
benchmark 1	2	1	0.5	1	0.1	1	1×10^{-3}
benchmark 2	3	1	0.5	1	0.1	3	1×10^{-3}
sandstone	4	7.7×10^{9}	0.1×10^{6}	2650	0.04	100	5×10^{-3}
cement paste	5	11.3×10^{9}	1.8×10^{6}	1500	0.253	23.8×10^{3}	1×10^{-3}
concrete	6	37.3×10^{9}	33.5×10^{6}	2450	1.4	300×10^{3}	1×10^{-3}

Preprints.org (www.preprints.org) | NOT PEER-REVIEWED | Posted: 1 April 2025 doi:10.20944/preprints202504.0083.v1

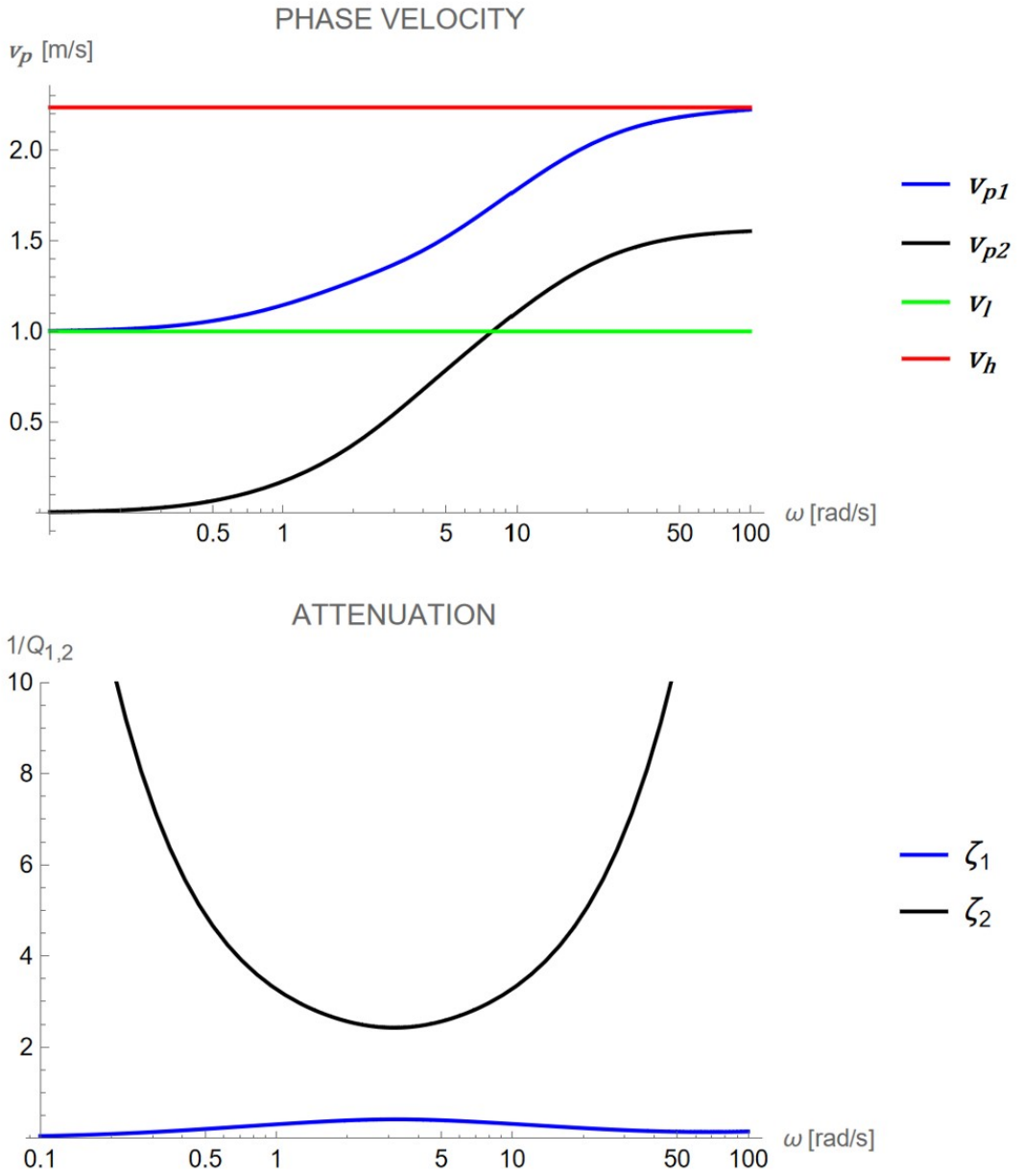

Figure 2. *Phase velocity v_p (m/s) and damping ratio as functions of the frequency ω (rad/s) according to equations (18) and (19) for a given material with constitutive parameters as shown in Table 1. The characteristic frequency, at which the attenuation peak can be distinguished, is 3.2 rad/s. The two asymptotes defined in equations (20) and (21) are also represented.*

 doi:10.20944/preprints202504.0083.v1

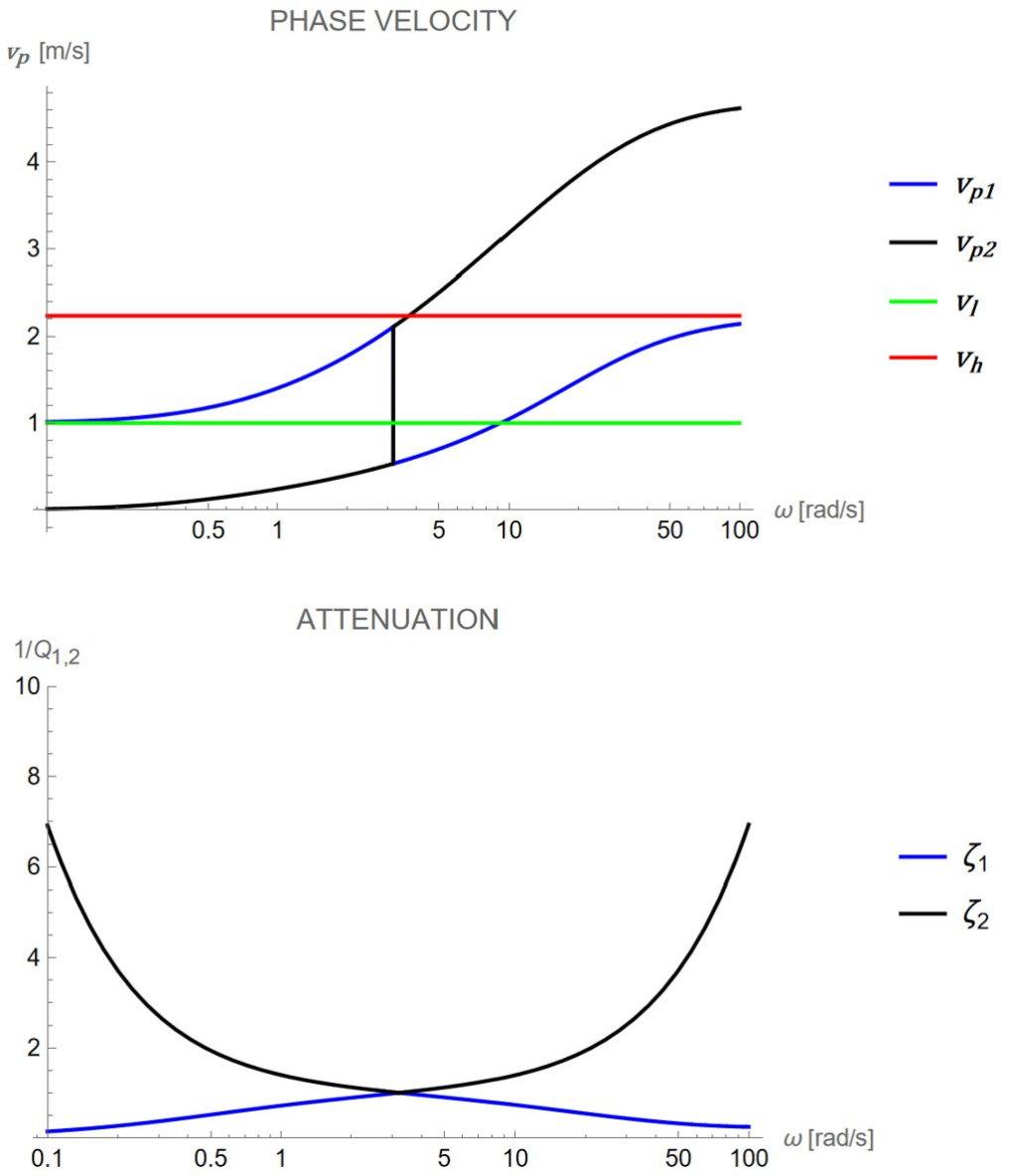

Figure 3. *Phase velocity v_p (m/s) and damping ratio as functions of the frequency ω (rad/s) according to equations (18) and (19) for a given material with constitutive parameters as shown in Table 1. The point at which the velocity jump occurs corresponds to the common peak, respectively maximum and minimum, of the two wave signals. The two asymptotes defined in equations (20) and (21) are also represented.*

Preprints.org (www.preprints.org) | NOT PEER-REVIEWED | Posted: 1 April 2025 doi:10.20944/preprints202504.0083.v1

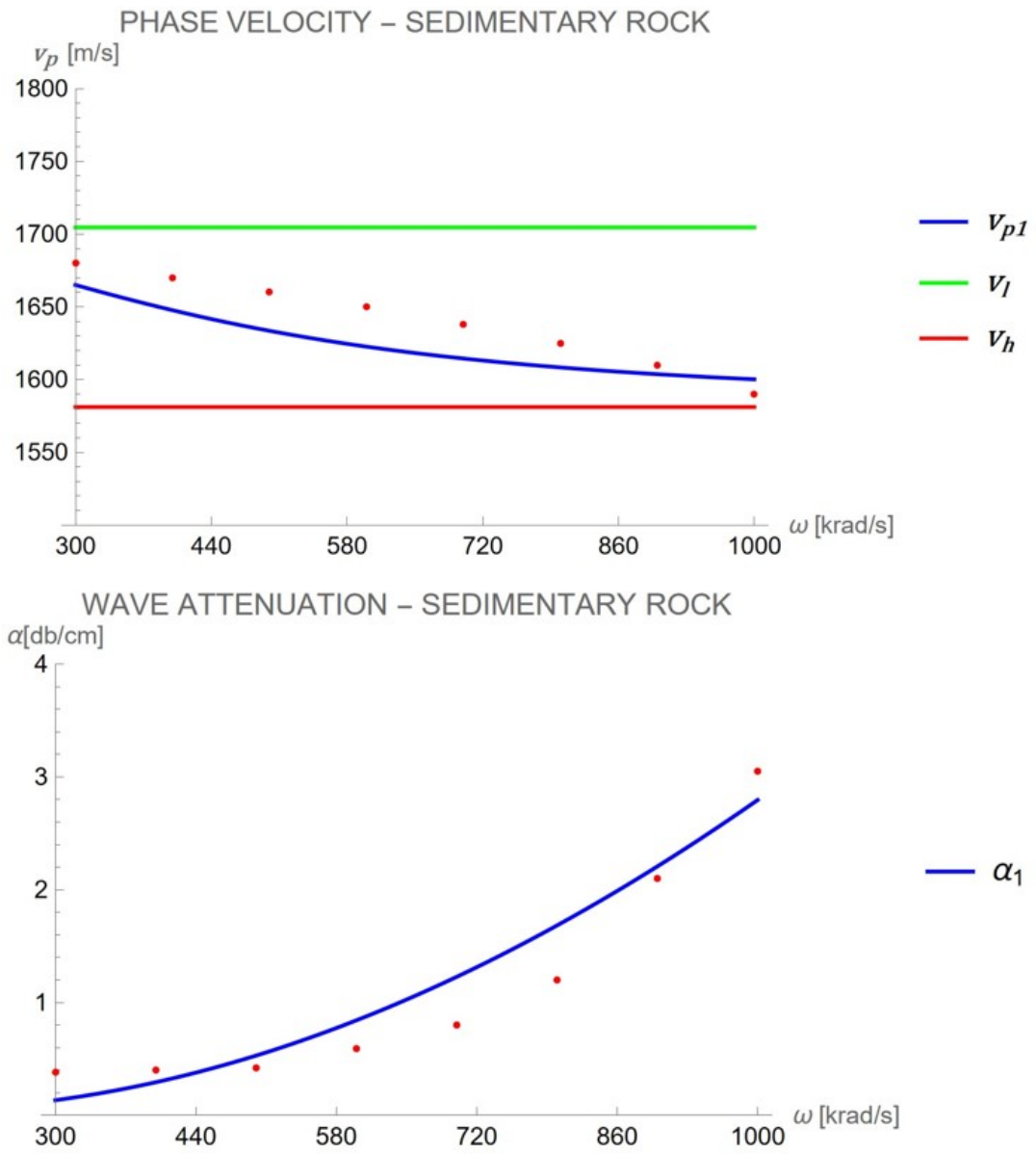

Figure 4. *Phase velocity v_p (m/s) and attenuation coefficient as functions of the frequency ω (rad/s) according to equations (18) and (23) for a sedimentary rock with constitutive parameters as shown in Table 1. Red points represent the experimental data by literature.*

 doi:10.20944/preprints202504.0083.v1

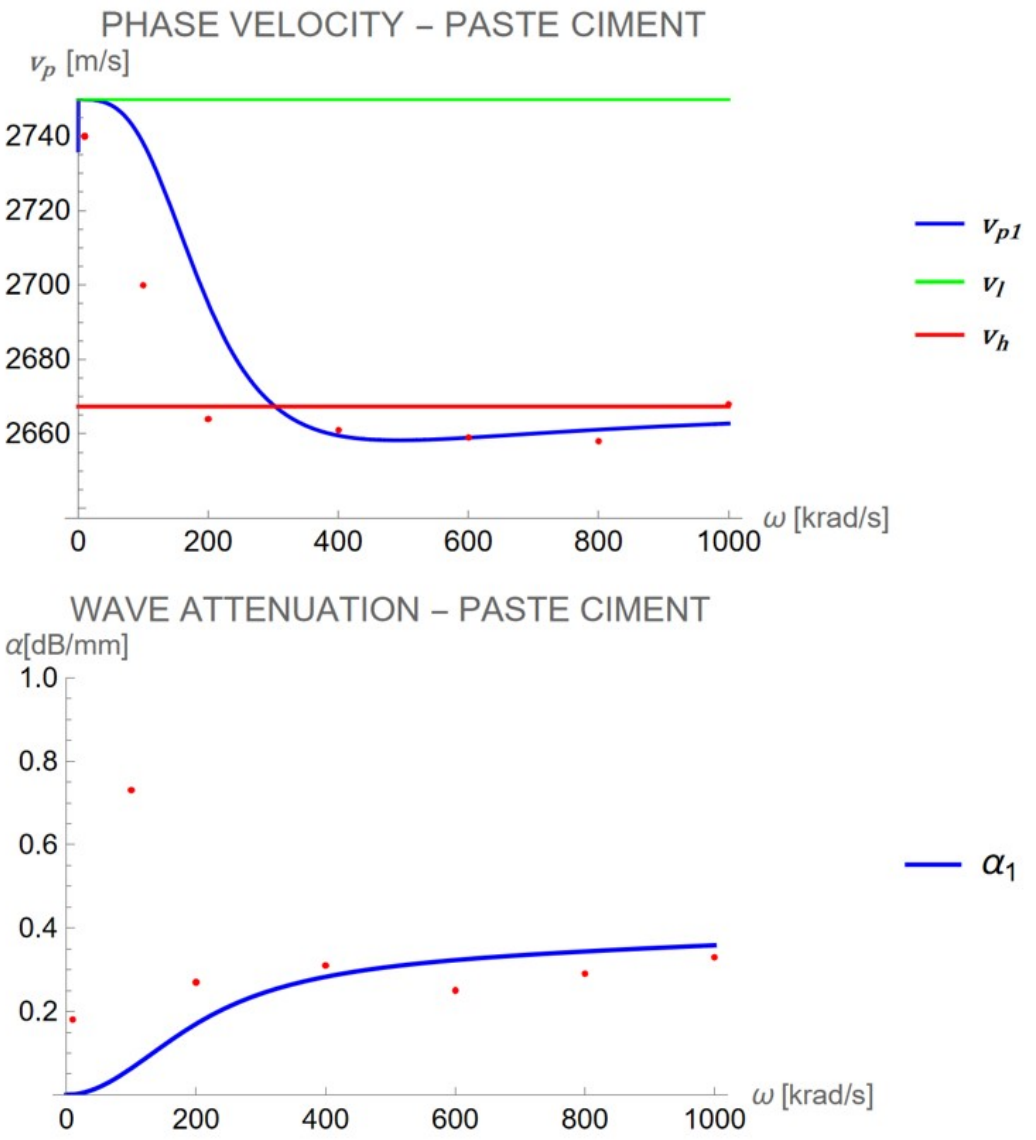

Figure 5. *Phase velocity v_p (m/s) and attenuation coefficient as functions of the frequency ω (rad/s) according to equations (18) and (23) for a paste cement sample with constitutive parameters as shown in Table 1. Red points represent the experimental data by literature.*

Preprints.org (www.preprints.org) | NOT PEER-REVIEWED | Posted: 1 April 2025 doi:10.20944/preprints202504.0083.v1

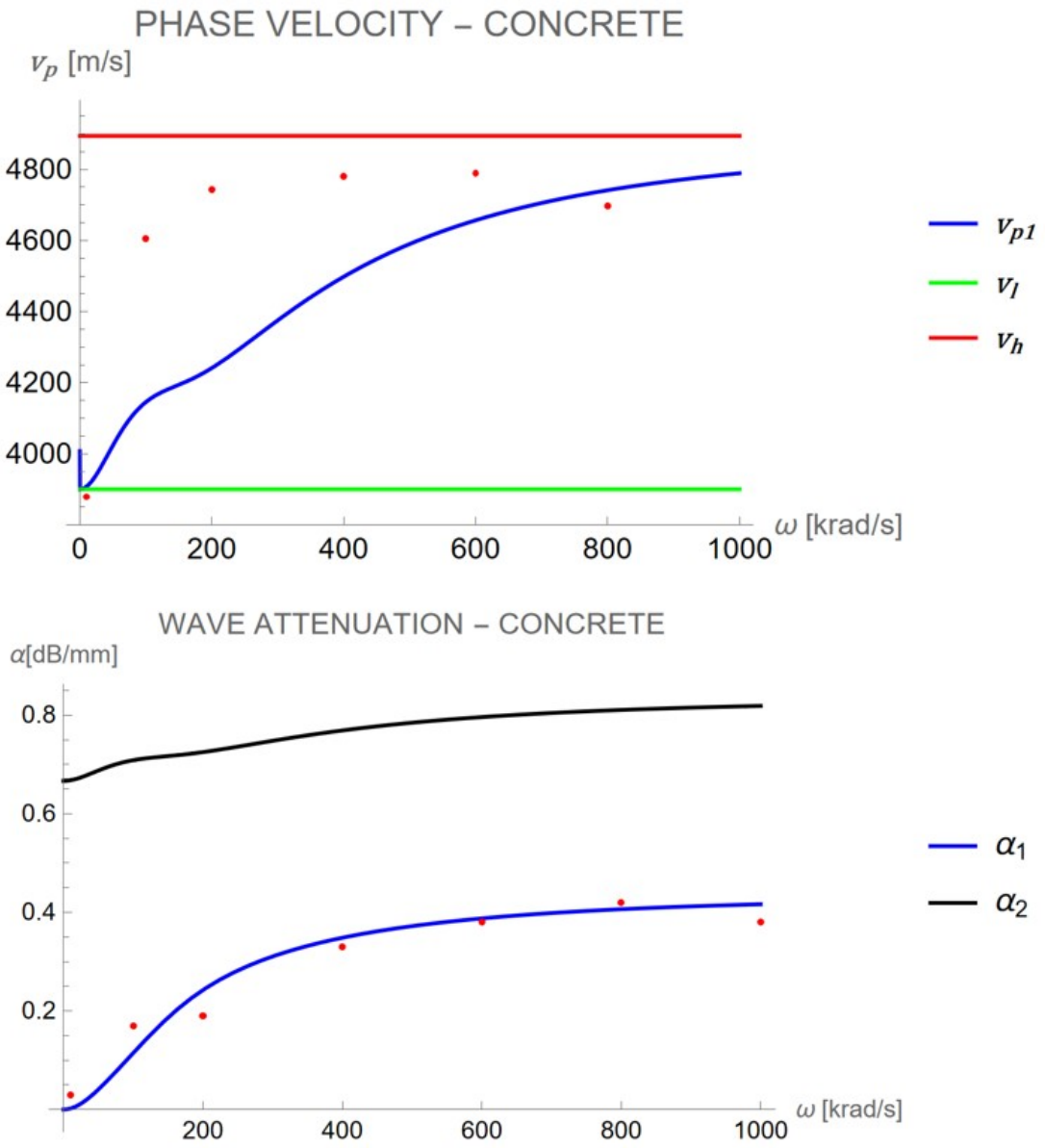

Figure 6. *Phase velocity v_p (m/s) and attenuation coefficient as functions of the frequency ω (rad/s) according to equations (18) and (23) for a concrete sample with constitutive parameters as shown in Table 1.Red points represent the experimental data by literature.*

3.2. Numerical Simulation Toward to the Benchmark

In Figure 2, we show for the numbers explained in Table 1 a graphical representation of the two phase velocities (18) and their respective attenuations (19) for the same values of the material characteristics present in Table 1. For c_1 and c_2 equal to zero, v_{p2} is zero, while v_{p1} asymptotically tends to the velocities for low-frequency regime v_l and for the high-frequency regime v_h as follows:

$$\lim_{\omega\to 0}\lim_{c_1\to 0}\lim_{c_2\to 0} v_{p_{1,2}} = v_l = \sqrt{\frac{k_1}{\rho}}, \tag{20}$$

$$\lim_{\omega\to \infty}\lim_{c_1\to 0}\lim_{c_2\to 0} v_{p_{1,2}} = v_h = \sqrt{\frac{k_2}{\eta}}, \tag{21}$$

For c_1 and c_2 different from zero, we observe in Figure 2 that the wave with phase velocity v_{p2} has a much higher attenuation than the wave with phase velocity v_{p1}, thus making it experimentally

 doi:10.20944/preprints202504.0083.v1

unmeasurable. Moreover, the variation of velocity from low to high frequency regimes occurs at a characteristic frequency for both waves, corresponding to the attenuation peak. For certain values of the viscosities c_1 and c_2, we can observe, as shown in Figures 3, a jump in the values of the phase velocities v_{p_1} and v_{p_2}, at the frequency at which the attenuation curves of the two signals exhibit a common peak. Nevertheless, the phase velocity measurable by ultrasonic instruments will be in all the cases the one with the lower attenuation, that is, v_{p_1} in the numerical example considered.

3.3. Validation with Data from Literature

Since experimental attenuation measurements available in the literature are generally expressed as the loss of signal amplitude between one end and the other of the sample along its length L and are measured in (dB/m), it is useful to introduce an attenuation coefficient, according the following formulation[12]:

$$\alpha = -\frac{20}{x} \cdot \log(\frac{u_x}{u_0}), \tag{22}$$

Replacing (15) into (22), using the Eulero proprieties and considering the real part and the imaginary part of the wavenumber, we obtain:

$$\alpha = -20ik_\omega \approx 20\mathrm{Im}(k_\omega), \tag{23}$$

where in the wavenumber we can omit the real part since, due to the fact we use maxim values of amplitude in (23), the cosine of the wavenumber, corresponding to the its real part, assume values for sure lower than those referred to the imaginary part. Once the material stiffness parameters, microstructure, micro-inertias, and density are set, the next step is to evaluate how variations in the internal viscosity of the material influence the combination of parameters that best approximate the experimental data for phase velocity and attenuation.

3.3.1. 1st Case of Study: Sandstone

The sediment specimen was prepared in a 100 mm × 100 mm × 50 mm container immersed in water to optimize velocity dispersion and minimize ultrasonic pulse attenuation [12]. The experiment took place in a 650 mm × 750 mm × 1500 mm water bath, using two matched pairs of broadband transducers with center frequencies of 0.5 MHz and 1.0 MHz[12]. The transducers were aligned coaxially with a 150 mm separation, mounted on a stable frame to ensure accurate wave amplitude measurements and prevent pressure variations on the probes [12] . In this case of study we know already the bulk modulus of the material and its density, so the phase velocity for low regime frequency is immediately obtained by equation (20). The values of microstructure and micro-inertia can be derived by calculating the characteristic length of the material, taking in account the fact that the velocity in the high-frequency regime is lower than that in the low-frequency regime according experimental data. In Figure 4, we present the overlap between numerical simulation, using the constitutive parameters of Table 1, and experimental data for phase velocity and wave attenuation in the tested material. In the frequency range of investigation, no attenuation peak is observed. The monotone trend observed in both phase velocity (decreasing) and attenuation (increasing) is successfully captured by the numerical simulation, confirming the model's accuracy in describing wave propagation behavior.

3.3.2. 2nd Case of Study: Cement Paste

The specimens tested were cubic of 150 mm edge, the experimental setup is a simple through-transmission ultrasonic configuration, using a waveform generator board and two broadband transducers of frequency between 300 kHz and 1 MHz, and a data acquisition system [13]. We consider the data for a sample with ratio water/ciment=0.375[13]. In Figure 5 we can compare experimental data with model numerical simulation. The velocity phase suddenly decreases (at 200 kHz) till to tend to the velocity for high frequency regime; in the attenuation graphic we observe the increasing trend, although a resonance peak can be observed at 100 kHz in the experimental data, probably due to other

 doi:10.20944/preprints202504.0083.v1

effects not included in the model as internal micro-fractures with inclusion of fluids or a measurement error.

3.3.3. 3rd Case of Study: Concrete

As for the cement paste, the specimens tested were cubic of 150 mm edge, and the experimental setup was the same of previous case of study [13]. Several different compositions of concrete were manufactured in function of water to cement ratio and of aggregate to cement ratio for a total of 24 specimens[13]. We consider the data for a sample with ratio water/ciment=0.375 [13]. Also in this case the model confirms the monotone trend of the experimental data[13].

4. Conclusions

The limitations of classical methods for the dynamic identification of material constitutive parameters, as well as the need for simple and reliable models capable of interpreting both dissipation and dispersion phenomena in wave propagation, are well-known issues[11]. Wave dispersion in materials under dynamic conditions has been extensively investigated in recent scientific literature [14–28]. Additionally, the effects of wave dissipation, starting from the wave amplitude value, have been the subject of many reference studies for this work[29–38]. Once the wave propagation has been reconstructed in terms of both dispersion and attenuation, excluding singular points such as cavities or localized heterogeneities, we know the variation of the phase velocity and wave amplitudes across the entire frequency spectrum and can also characterize them in classical terms[11,13,39,40]. With this study we have formulated and validated a theoretical model that allows us to characterize, for a given material, both the dispersion and attenuation of the ultrasonic wave propagating through it, as well as all the key constitutive parameters associated with ultrasonic propagation (mechanical stiffness, microstructure, internal viscosity). The models has been constructed by applying the principle of Hamilton-Raylegh [41,42] and for the sake of simplicity, a one-dimensional model and only the longitudinal elastic modulus have been considered, whereas for the future a more in-depth investigation can take into account also 3D effects and therefore all the relevant elastic parameters.

Author Contributions: Conceptualization, De Fazio, N., Placidi,L., Fabbrocino, F., Luciano, R.; methodology, Placidi, L., Fabbrocino, F., Luciano, R.; software, De Fazio, N.; validation, De Fazio, N.; formal analysis, De Fazio, N.; investigation, De Fazio, N.; resources, De Fazio, N.; data curation, De Fazio, N.; writing—original draft preparation, De Fazio, N.; writing—review and editing, Placidi, L., Fabbrocino, F., Luciano, R.; visualization, Placidi, L.; supervision, Placidi, L.; project administration, Placidi, L.. All authors have read and agreed to the published version of the manuscript.

Funding: This research received no external funding.

Informed Consent Statement: Not applicable.

Data Availability Statement: Data available in a publicly accessible repository.

Conflicts of Interest: The authors declare no conflicts of interest.

Abbreviations

The following abbreviations are used in this manuscript:
Legend of Symbols and Their Meanings

Symbol	Mean
$A(u)$	Action functional
K	Kinetic energy density
W^{int}	Potential energy density
W^{ext}	External energy
x	Position in the reference configuration
t	Time

 doi:10.20944/preprints202504.0083.v1

t_0, t_1	Two instants of time
L	Length of the 1D model in the reference configuration
$u(x,t)$	Displacement field
k_1	Standard material elastic modulus
k_2	Non-standard strain gradient material elastic modulus
ρ	Mass density
η	Micro-inertia
F_y^{ext}	Concentrated forces applied at $x = y$
B_y^{ext}	Concentrated double forces applied at $x = y$
δ	Variation operator
b_n	Distributed forces
b_d	Distributed double forces
u_0	Complex wave amplitude
k_w	Wave number
$\hat{k}_w$	Wave number for right-hand direction propagative wave
ω	Wave frequency
i	Imaginary unit
Re	Real operator
Im	Imaginary operator
v_p	Plane wave velocity phase
v_l	Low frequency regime velocity
v_h	High frequency regime velocity
c_1	Internal material viscosity related to first gradient field
c_2	Internal material viscosity related to second gradient field
R	Rayleigh function
Q	Quality factor
ζ	Damping ratio
α	Attenuation coefficient

References

1. Aifantis, E.C. The Role of Gradient in the Mechanics of Materials. *Journal of Elasticity* **2003**, *72*, 177–200.
2. Steigmann, D.J. The mechanics of second-gradient materials. *Journal of Elasticity* **2002**, *72*, 1–12. https://doi.org/10.1023/A:1014282717639.
3. Germain, P. The Mechanics of Materials with Second-Order Gradients. *Journal of the Mechanics and Physics of Solids* **1973**, *21*, 489–509.
4. Eshelby, J.D. Elastic Inclusions and the Theory of Composite Materials. *Journal of Elasticity* **1980**, *10*, 319–343.
5. Pendry, J.B. Metamaterials: The First Hundred Years. *Science* **2006**, *314*, 230–231.
6. Bauchau, P. Ultrasonic Wave Propagation in Biological Tissues. *The Journal of the Acoustical Society of America* **2001**, *110*, 2417–2424.
7. Jafferis, J. Non-local Effects and Attenuation in Wave Propagation. *Journal of Applied Physics* **2015**, *89*, 283–299.
8. Lurie, D. Viscoelastic Effects in Second-Gradient Materials: A Theoretical Framework. *Journal of Mechanics and Physics of Solids* **2017**, *102*, 37–50. https://doi.org/10.1016/j.jmps.2017.01.004.
9. Bucur, D. *Non-Destructive Testing of Materials by Ultrasonic Waves*; Springer, 2010.
10. Hofmann, R. Frequency Dependent Elastic and Anelastic Properties of Clastic Rocks. *Thesis degree by Colorado School of Mines* **2006**, p. 185.
11. Lauwerier, H.A.; Koiter, W.T. North-Holland Series on Applied Mathematics and Mechanics. *North-holland Series in Applied Mathematics and Mechanics* **1967**, *2*.
12. Lee, K.; Humphrey, V.; Kim, B.N.; Yoon, S. Frequency dependencies of phase velocity and attenuation coefficient in a water-saturated sandy sediment from 0.3 to 1.0 MHz. *The Journal of the Acoustical Society of America* **2007**, *121*, 2553–8. https://doi.org/10.1121/1.2713690.
13. Philippidis, T.; Aggelis, D. Experimental study of wave dispersion and attenuation in concrete. *Ultrasonics* **2005**, *43*, 584–95. https://doi.org/10.1016/j.ultras.2004.12.001.
14. Mace, B.; Marconi, E. Wave motion and dispersion phenomena: Veering, locking and strong coupling effects. *The Journal of the Acoustical Society of America* **2012**, *131*, 1015–1028.

 doi:10.20944/preprints202504.0083.v1

15. di Marzo, M.; Tomassi, A.; Placidi, L. A Methodology for Structural Damage Detection Adding Masses. *Research in Nondestructive Evaluation* **2024**, *35*, 172–196.
16. Wolfenden, A. *Dynamic Elastic Modulus Measurements in Materials*; ASTM International, 1990.
17. Giorgio, I.; Della Corte, A.; Dell'Isola, F. Dynamics of 1D nonlinear pantographic continua. *Nonlinear Dynamics* **2017**, *88*, 21–31.
18. Yang, B.; Bacciocchi, M.; Fantuzzi, N.; Luciano, R.; Fabbrocino, F. Computational simulation and acoustic analysis of two-dimensional nano-waveguides considering second strain gradient effects. *Computers & Structures* **2024**, *296*, 107299.
19. Yang, B.; Fantuzzi, N.; Bacciocchi, M.; Fabbrocino, F.; Mousavi, M. Nonlinear wave propagation in graphene incorporating second strain gradient theory. *Thin-Walled Structures* **2024**, *198*, 111713.
20. Laudato, M.; Barchiesi, E., Non-linear dynamics of pantographic fabrics: modelling and numerical study. In *Wave Dynamics, Mechanics and Physics of Microstructured Metamaterials: Theoretical and Experimental Methods*; 2019; pp. 241–254.
21. Nejadsadeghi, N.; Misra, A. Role of Higher-order Inertia in Modulating Elastic Wave Dispersion in Materials with Granular Microstructure. *International Journal of Mechanical Sciences* **2020**, *185*, 105867.
22. Dell'Isola, F.; Madeo, A.; Placidi, L. Linear plane wave propagation and normal transmission and reflection at discontinuity surfaces in second gradient 3D continua. *ZAMM-Journal of Applied Mathematics and Mechanics/Zeitschrift für Angewandte Mathematik und Mechanik* **2012**, *92*, 52–71.
23. dell'Isola, F.; Eugster, S.R.; Fedele, R.; Seppecher, P. Second-gradient continua: From Lagrangian to Eulerian and back. *Mathematics and Mechanics of Solids* **2022**, *27*, 2715–2750.
24. Shekarchizadeh, N.; Laudato, M.; Manzari, L.; Abali, B.E.; Giorgio, I.; Bersani, A.M. Parameter identification of a second-gradient model for the description of pantographic structures in dynamic regime. *Zeitschrift für angewandte Mathematik und Physik* **2021**, *72*, 190.
25. Giorgio, I.; Andreaus, U.; Dell'Isola, F.; Lekszycki, T. Viscous second gradient porous materials for bones reconstructed with bio-resorbable grafts. *Extreme Mechanics Letters* **2017**, *13*, 141–147.
26. Madeo, A.; Dell'Isola, F.; Darve, F. A continuum model for deformable, second gradient porous media partially saturated with compressible fluids. *Journal of the Mechanics and Physics of Solids* **2013**, *61*, 2196–2211.
27. Dell'Isola, F.; Hutter, K. Variations of porosity in a sheared pressurized layer of saturated soil induced by vertical drainage of water. *Proceedings of the Royal Society of London. Series A: Mathematical, Physical and Engineering Sciences* **1999**, *455*, 2841–2860.
28. Luciano, R.; Barbero, E. Formulas for the stiffness of composites with periodic microstructure. *International Journal of Solids and Structures* **1994**, *31*, 2933–2944. https://doi.org/https://doi.org/10.1016/0020-7683(94)90060-4.
29. Fabbrocino, F.; Amendola, A. Discrete-to-continuum approaches to the mechanics of pentamode bearings. *Composite Structures* **2017**, *167*, 219–226.
30. Fabbrocino, F.; Carpentieri, G. Three-dimensional modeling of the wave dynamics of tensegrity lattices. *Composite Structures* **2017**, *173*, 9–16.
31. Ciallella, A.; Giorgio, I.; Eugster, S.R.; Rizzi, N.L.; dell'Isola, F. Generalized beam model for the analysis of wave propagation with a symmetric pattern of deformation in planar pantographic sheets. *Wave Motion* **2022**, *113*, 102986.
32. Barchiesi, E.; Laudato, M.; Di Cosmo, F. Wave dispersion in non-linear pantographic beams. *Mechanics Research Communications* **2018**, *94*, 128–132.
33. Abali, B.E.; Vazic, B.; Newell, P. Influence of microstructure on size effect for metamaterials applied in composite structures. *Mechanics Research Communications* **2022**, *122*, 103877.
34. Migliaccio, G.; D'Annibale, F. On the role of different nonlinear damping forms in the dynamic behavior of the generalized Beck's column. *Nonlinear Dyn* **2024**, *112*, 13733–13750. https://doi.org/10.1007/s11071-024-09825-z.
35. Placidi, L.; Di Girolamo, F.; Fedele, R. Variational study of a Maxwell–Rayleigh-type finite length model for the preliminary design of a tensegrity chain with a tunable band gap. *Mechanics Research Communications* **2024**, *136*, 104255.
36. Berezovski, A.; Giorgio, I.; Corte, A.D. Interfaces in micromorphic materials: wave transmission and reflection with numerical simulations. *Mathematics and Mechanics of Solids* **2016**, *21*, 37–51.
37. Placidi, L.; Rosi, G.; Giorgio, I.; Madeo, A. Reflection and transmission of plane waves at surfaces carrying material properties and embedded in second-gradient materials. *Mathematics and Mechanics of Solids* **2014**, *19*, 555–578.

 doi:10.20944/preprints202504.0083.v1

38. Hima, N.; D'Annibale, F.; Dal Corso, F. Non-smooth dynamics of buckling based metainterfaces: rocking-like motion and bifurcations. *International Journal of Mechanical Sciences* **2023**, *242*, 108005.
39. Varadan, V.K.; Varadan, V.V.; Ma, Y. Frequency-dependent elastic properties of rubberlike materials with a random distribution of voids. *The Journal of the Acoustical Society of America* **1984**, *76*, 296–300.
40. Rosi, G.; Placidi, L.; Auffray, N. On the validity range of strain-gradient elasticity: a mixed static-dynamic identification procedure. *European Journal of Mechanics-A/Solids* **2018**, *69*, 179–191.
41. dell'Isola, F.; Placidi, L. Variational principles are a powerful tool also for formulating field theories. International Research Centre on "Mathematics Mechanics of Complex Systems" M&MOCS, 2013.
42. Abali, B.E. Revealing the physical insight of a length-scale parameter in metamaterials by exploiting the variational formulation. *Continuum Mechanics and Thermodynamics* **2019**, *31*, 885–894.